ORIGINAL ARTICLE

Anti-lymphangiogenic diterpenes from the bark of *Calocedrus macrolepis var. formosana*

Tzong-Huei Lee [a,1], Chin-Lin Hsieh [b,c], Ho-Cheng Wu [a], Shih-Wei Wang [d,e,f], Chen-Lin Yu [d,e], George Hsiao [g], Ming-Jen Cheng [h], Wen-Tsong Hsieh [i,1], Yueh-Hsiung Kuo [j,k,l,*]

[a] Institute of Fisheries Science, National Taiwan University, Taipei, 106, Taiwan
[b] Department of Chemistry, National Taiwan University, Taipei, 106, Taiwan
[c] Department of Disaster Management, Taiwan Police College, Taipei, 116, Taiwan
[d] Institute of Biomedical Sciences, MacKay Medical College, New Taipei City, 252, Taiwan
[e] Department of Medicine, Mackay Medical College, New Taipei City, 252, Taiwan
[f] Graduate Institute of Natural Products, College of Pharmacy, Kaohsiung Medical University, Kaohsiung, Taiwan
[g] Graduate Institute of Medical Sciences, College of Medicine, Taipei Medical University, Taipei, Taiwan
[h] Bioresource Collection and Research Center (BCRC), Food Industry Research and Development Institute (FIRDI), Hsinchu, 300, Taiwan
[i] Department of Pharmacology, China Medical University, Taichung, 404, Taiwan
[j] Department of Chinese Pharmaceutical Sciences and Chinese Medicine Resources, China Medical University, Taichung, 404, Taiwan
[k] Chinese Medicine Research Center, China Medical University, Taichung, 404, Taiwan
[l] Department of Biotechnology, Asia University, Taichung, 413, Taiwan

Abstract

Eight new diterpenes, 6α,7β-dihydroxyferruginol (1), 6α,7α-dihydroxyferruginol (2), 6α-hydroxyhinokiol (3), 4α-hydroxy-7-oxo-18-norabieta-8,11,13-trien-4α-ol (4a), 15,16-dehydrosugiol (5), 7-methoxy-6,7-secoabieta-8,11,13-triene-6,12-diol (6), 7α-acetoxyabieta-8,12-diene-11,14-dione (7), 7α-butyloxyethyloxyabieta-8,12-diene-11,14-dione (8), along with four known compounds, 6,7-dehydroferruginol (9), 12-hydroxy-6,7-secoabieta-8,11,13-triene-6,7-dial (10), 7α-11-dihydroxy-12-methoxy-8,11,13-abietatriene (11), and 11,14-dihydroxy-8,11,13-abietatrien-7-one (12) were successfully isolated from the bark of *Calocedrus macrolepis var. formosana*. The structures of all isolates were elucidated by physical data (appearance, UV, IR, optical rotation) and spectroscopic data (1D, 2D NMR, and HREIMS). Compounds 9, 10, 11, and 12 showed promising growth-inhibitory effect on human lymphatic endothelial cells (LECs). Among these compounds, compound 10 exerted the most potent anti-lymphangiogenesis property by suppressing cell growth and tube formation of LECs. In conclusion, the results revealed the anti-lymphangiogenic potentials of Formosan *C. macrolepis var. formosana.*

Keywords: Anti-lymphangiogenesis, *Calocedrus macrolepis var.formosana*, Diterpenes

1. Introduction

Cancer is one of the largest health problems across the world. According to the GLOBOCAN, 18.1 million new cancer cases were diagnosed and 9.6 million cancer-related deaths in 2018 [1]. Although there are many types of cancer treatment, the common types of anti-cancer options such as chemotherapy and radiotherapy usually have severe side effects, causing low medication adherence and treatment failure. The high mortality rates of cancer patients are not only associated with the occurrence of primary tumors but, highly by the metastatic spread of tumor cells from the original site to other organs [2]. In the tumor microenvironment, primary tumors will secrete growth factors

Received 4 June 2021; accepted 18 August 2021.
Available online ■ ■ ■

* Corresponding author at: Department of Chinese Pharmaceutical Sciences and Chinese Medicine Resources, China Medical University, No. 100, Sec. 1, Jingmao Rd., Taichung, 404, Taiwan.
E-mail address: kuoyhlab@gmail.com (Y.-H. Kuo).
[1] These authors contributed equally to this work.

https://doi.org/10.38212/2224-6614.3375

to format new lymphatic vessels and help cancer cells disseminates to other lymph node [3]. Thus, the development of a target cancer therapy with anti-lymphangiogenic activity is an effective strategy for improving patient survival rates.

The *Calocedrus* species (Cupressaceae) comprises three species with acceptable names, mainly distributed in western north American, Taiwan, and southwestern China [4]. The major component, hinokiol, and other physico-chemical properties of this plant improves the resistance to decay and wood durability [5,6]. Previous studies of *Calocedrus macrolepis* Kurz var. *formosana* (Florin) W. C. Cheng & L. K. Fu identified various classes of chemical constituents, such as fatty acids, monoterpenes, shonanic acids [7–9], sesquiterpenes [10], diterpenes [4,11–15], furanones [10], sesquarterpene (C_{35}) [16,17], and lignans [4]. Some of them showed cytotoxicity [4,16–18], anti-inflammatory [19], antioxidant [19,20], anti-microbial [20], anti-plant pathogenic fungi [21], and arteriosclerosis prevention [14] activity. Our long-term studies on the *C. macrolepis var. formosana* have identified plentiful secondary metabolites with cytotoxicity toward human oral epidermoid carcinoma KB cells [13,16,17], which prompted us to further explore its ingredients as the source of cytotoxic compounds.

With a series of isolation and purification process, we successfully isolated twelve diterpenes from the bark of *C. macrolepis var. formosana* in current study. Diterpenoids are well-known for its cytotoxicity toward different kind of tumors. Surprisingly, diterpenes exhibited anti-lymphangiogenic activity, a novel concept for targeting tumor cell metastasis in previous investigation [22]. Thus, to confirm the relationship between diterpenes and anti-lymphangiogenic activity, as well as to broaden the pharmacological property of diterpenes, the anti-lymphangiogenic activity of isolated compounds in this study was evaluated. Here, we report the structure elucidation of eight new diterpenes along with four known compounds from the bark of *C. macrolepis var. formosana* (Fig. 1). Among these, compounds **9**, **10**, **11**, and **12** exhibited anti-lymphangiogenic activity.

2. Materials and methods

2.1. General experimental procedures

Optical rotations were measured on a Jasco DIP-1000 Digital polarimeter (Jasco, Kyoto, Japan), and IR spectra (neat) were acquired with a Perkin-Elmer 983G spectrometer (Perkin-Elmer, Waltham, MA, USA). The 1D (^{1}H, ^{13}C, DEPT) and 2D (COSY, NOESY, ROESY, HSQC, HMBC) NMR spectra were obtained from a Burcher DMX-500 spectrometer (Bruker Inc., Bremen, Germany) operated at 500 (^{1}H) and 125 MHz (^{13}C). The HRESIMS data were generated at the Mass Spectrometry Laboratory by a JEOL JMS-H110 mass spectrometer (FAB-MS) (JEOL, Inc. Tokyo, Japan). Extracts were chromatographed on silica gel (Merk 70–230 mesh, 230–400 mesh, ASTM) and purified with a semipreparative normal-phase HPLC column (Merck LichroCART 250 × 10 mm, 7 μm, LiChrosorb Si 60) taken on LDC Analytical-III.

2.2. Plant materials

The dried bark of *C. macrolepis* var. *formosana* was collected in Nan-Tou, Taiwan (Aug., 1998) and identified by Prof. Shang-Tzen Chang in the Department of Forestry, National Taiwan University. A voucher specimen (No. 223133) has been deposited in the Herbarium of the Department of Life Science, National Taiwan University, Taipei, Taiwan.

2.3. Extraction and isolation

The dried bark of *C. macrolepis* var. *formosana* (16 kg) was extracted with acetone (140 L) at room temperature (two times, 7 days/each time). The acetone extract (1.8 kg) was suspended in H_2O, then partitioned with EtOAc. The EtOAc layer (734 g) was subjected to open column chromatography (SiO_2 60, 70–230 mesh; Merck), and purified by repeated normal-phase HPLC with mixtures of *n*-hexane and EtOAc as eluents. Compounds **2** (H/E = 6:4, 2.4 mg), **3** (H/E = 6:4, 1.5 mg), **4a** (H/E = 7:3, 2.1 mg), **5** (H/E = 4:1, 1.5 mg), **6** (H/E = 4:1, 1.9 mg), **7** (H/E = 7:3, 2.0 mg), **8** (H/E = 9:1, 2.2 mg), **9** (H/E = 4:1, 1.3 mg), **10** (H/E = 7:3, 4.5 mg), **11** (H/E = 4:1, 9.3 mg), **12** (H/E = 6:4, 6.3 mg), and **13** (H/E = 9:1, 10.2 mg) were obtained using above solvent systems as mobile phase, respectively.

2.4. Spectral data

*6α,7β-Dihydroxyferruginol (**1**):* Gum; $[\alpha]_D^{25}$ +35.1 (*c* 0.2, acetone); UV (MeOH) λ_{max} (log ϵ) 235 (3.39), 280 (3.23) nm; IR (neat) υ_{max} 3365, 1617, 1582, 1500, 1462 cm^{-1}; HREIMS *m/z* 318.2197 $[M]^+$ (calcd. for $C_{20}H_{30}O_3$ 318.2195); ^{1}H (500 MHz, acetone-d_6) and ^{13}C NMR (125 MHz, acetone-d_6): see Tables 1 and 2.

*6α,7α-Dihydroxyferruginol (**2**):* Gum; $[\alpha]_D^{25}$ +25.7 (*c* 0.5, acetone); UV (MeOH) λ_{max} (log ϵ) 225 (3.67), 283 (3.25) nm; IR (neat) υ_{max} 3367, 1618, 1582, 1508 cm^{-1}; HREIMS *m/z* 318.2197 $[M]^+$ (calcd. for $C_{20}H_{30}O_3$ 318.2196); ^{1}H (500 MHz, acetone-d_6) and ^{13}C NMR (125 MHz, acetone-d_6): see Tables 1 and 2.

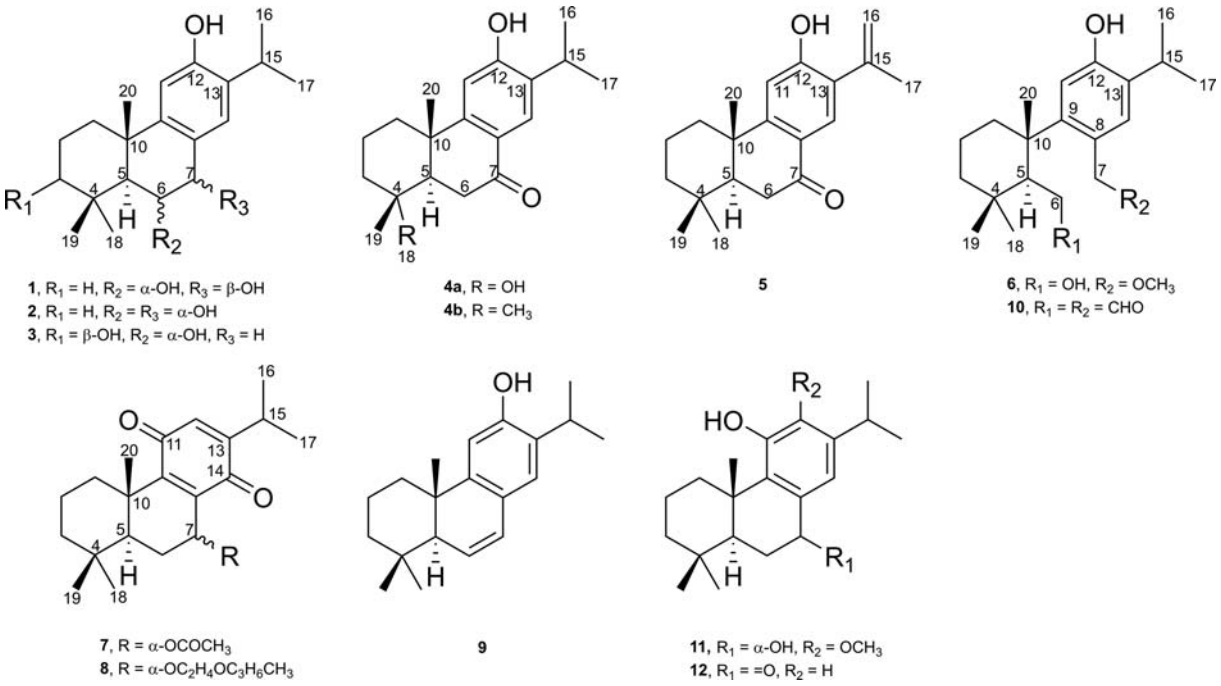

*Fig. 1. Chemical structures of compounds **1**–**12**.*

6α-Hydroxyhinokiol (3): Gum; $[\alpha]_D^{25}$ +9.0 (*c* 0.54, MeOH); UV (MeOH) λ_{max} (log ϵ) 218 (3.67), 280 (3.31) nm; IR (neat) υ_{max} 3368, 1616, 1505 cm^{-1}; HREIMS *m/z* 318.2200 $[M]^+$ (calcd. for $C_{20}H_{30}O_3$ 318.2189); ^1H (500 MHz, acetone-d_6) and ^{13}C NMR (125 MHz, acetone-d_6): see Tables 1 and 2.

4α-Hydroxy-7-oxo-18-norabieta-8,11,13-trien-4α-ol (4a): Gum; $[\alpha]_D^{25}$ +5.1 (*c* 0.50, MeOH); UV (MeOH) λ_{max} (log ϵ) 231 (3.73), 281 (3.62) nm; IR (neat) υ_{max} 3335, 1654, 1596, 1503 cm^{-1}; HREIMS *m/z* 302.1881 $[M]^+$ (calcd. for $C_{19}H_{26}O_3$ 302.1876); ^1H (500 MHz, $CDCl_3$) and ^{13}C NMR (125 MHz, $CDCl_3$): see Tables 1 and 2.

15,16-Dehydrosugiol (5): Colorless solid; $[\alpha]_D^{25}$ +8.2 (*c* 0.4, MeOH); UV (MeOH) λ_{max} (log ϵ) 235 (3.99), 280 (3.83) nm; IR (KBr) υ_{max} 3099, 1642, 1581, 1500, 1491, 898, 870 cm^{-1}; HREIMS *m/z* 298.1927 $[M]^+$ (calcd. for $C_{20}H_{26}O_2$ 298.1934); ^1H (500 MHz, $CDCl_3$) and ^{13}C NMR (125 MHz, $CDCl_3$): see Tables 1 and 2.

7-Methoxy-6,7-secoabieta-8,11,13-triene-6,12-diol (6): Colorless solid; $[\alpha]_D^{25}$ −1.2 (*c* 0.19, MeOH); UV (MeOH) λ_{max} (log ϵ) 231 (3.57), 281 (3.08) nm; IR (KBr) υ_{max} 3368, 1614, 1582, 1485, 1442 cm^{-1}; HREIMS *m/z* 334.2503 $[M]^+$ (calcd. for $C_{21}H_{34}O_3$ 334.2509); ^1H (500 MHz, $CDCl_3$) and ^{13}C NMR (125 MHz, $CDCl_3$): see Tables 1 and 2.

7α-Acetoxyabieta-8,12-diene-11,14-dione (7): Yellowish solid; $[\alpha]_D^{25}$ −23.7 (*c* 0.2, MeOH); UV (MeOH) λ_{max} (log ϵ) 257 (3.92) nm; IR (KBr) υ_{max} 1731, 1650, 1603, 1461 cm^{-1}; HREIMS *m/z* 358.2151 $[M]^+$ (calcd. for $C_{22}H_{30}O_4$ 358.2145); ^1H (500 MHz, $CDCl_3$) and ^{13}C NMR (125 MHz, $CDCl_3$): see Tables 1 and 2.

7α-Butyloxyethyloxyabieta-8,12-diene-11,14-dione (8): Yellowish solid; $[\alpha]_D^{25}$ −10.5 (*c* 0.4, MeOH); UV (MeOH) λ_{max} (log ϵ) 256 (3.60) nm; IR (KBr) υ_{max} 1652, 1600, 1462 cm^{-1}; HREIMS *m/z* 416.2927 $[M]^+$ (calcd. for $C_{26}H_{40}O_4$ 416.2928); ^1H (500 MHz, $CDCl_3$) and ^{13}C NMR (125 MHz, $CDCl_3$): see Tables 1 and 2.

2.5. Anti-lymphangiogenic assay

The methods for cell culture, cell growth, tube formation, and cytotoxicity of human lymphatic endothelial cells were the same as our previous work [23].

3. Results and discussion

Compounds **1** and **2** were separable abietane-type diterpenoids with almost identical physical data (appearance, UV, IR, optical rotation) and spectroscopic properties including ^1H (Table 1), ^{13}C NMR spectra (Table 2), and HREIMS. They were obtained as gum with positive optical activity, and were assigned the same molecular formula as $C_{20}H_{30}O_3$ through analysis of the molecular ion $[M]^+$ at *m/z* 318.2197 (calcd. for $C_{20}H_{30}O_3$ 318.2195) in the HREIMS, which indicated six degrees of unsaturation. The following gross structure determination took compound **1** as an example, and determined the relative configuration of compounds **1** and **2** by NOESY interpretation and coupling constant. The IR spectrum of compound **1** showed absorptions at 3365 1617, 1582, and 1578 cm^{-1}, indicating the

*Table 1. The ^{1}H NMR data of compounds **1**–**3**, **4a**, and **5**–**8** in 500 MHz.*

	1[a]	2[a]	3[a]	4a[b]	5[b]	6[b]	7[b]	8[b]
Position	δ_H, mult (*J* in Hz)	δ_H, mult (*J* in Hz)	δ_H, mult (*J* in Hz)	δ_H, mult (*J* in Hz)	δ_H, mult (*J* in Hz)	δ_H, mult (*J* in Hz)	δ_H, mult (*J* in Hz)	δ_H, mult (*J* in Hz)
1	1.33, td (13.5, 3.6) 2.11, br d (13.5)	1.36, td (13.6, 3.7) 2.07, br d (13.6)	1.56, td (12.6, 5.1) 2.01, td (12.6, 3.4)	1.52, td (12.4, 3.4) 2.16, br d (12.4)	1.51, m 2.24, br d (12.7)	1.40, m 2.08, m	1.45, m 2.67, br d (13.1)	1.16, td (13.1, 3.3) 2.59, br d (13.1)
2	1.52, m 1.72, qt (13.6, 3.4)	1.56, br d (13.6) 1.72, qt (13.6, 3.4)	1.74–1.80, m	1.62–1.68, m 1.78–1.82, m	1.66, m 1.75, m	1.55, m 1.69, m	1.54, m 2.71, td (13.1, 3.2)	1.45, m 1.69, qt (13.1, 3.3)
3	1.27, td (13.6, 3.4) 1.40, br d (13.6)	1.23, td (13.6, 3.7) 1.44, br d (13.6)	3.18, m	1.41, td (13.4, 3.7) 1.89, br d (13.4)	1.24, m 1.54, m	1.53, m	1.16, m 1.45, m	1.23, m 1.40, m
5	1.44, d (11.3)	1.52, d (9.2)	1.15, m	2.08, dd (14.1, 3.5)	1.83, dd (13.8, 4.0)	2.17, m	1.42, m	1.58, m
6	4.04, dd (11.3, 7.2)	4.14, dd (9.2, 4.4)	4.31, m	2.55, dd (17.9, 3.5) 2.91, dd (17.9, 14.1)	2.58, dd (18.1, 13.8) 2.67, dd (18.1, 4.0)	3.40, m 3.55, br d	1.63, td (14.9, 4.1) 1.92, d (14.9)	1.40, m 2.02, br d (13.1)
7	4.42, d (7.2)	4.66, d (4.4)	2.66, dd (16.0, 3.5) 3.20, m			4.57, d (10.4) 4.70, br d (10.4)	5.91, t (4.1)	4.41, br d (3.6)
11	6.66, s	6.68, s	6.67, s	6.68, s	6.87, s	6.93, s		
14	7.28, s	7.21, s	6.82, s	7.91, s	7.85, s	7.15, s	6.38, s	6.32, s
15	3.22, sep (6.9)	3.24, sep (6.9)	3.21, sep (6.7)	3.12, sep (6.9)		3.22, sep (6.9)	2.97, sep (6.8)	2.98, sep (6.9)
16	1.18, d (6.9)	1.18, d (6.9)	1.18, d (6.7)	1.23, d (6.9)	5.11, br s 5.41, br s	1.19, d (6.9)	1.07, d (6.8)	1.05, d (6.9)
17	1.19, d (6.9)	1.20, d (6.9)	1.17, d (6.7)	1.25, d (6.9)	2.10, s	1.20, d (6.9)	1.09, d (6.8)	1.08, d (6.9)
18	1.23, s	1.01, s	1.20, s		0.91, s	1.06, s	0.85, s	0.92, s
19	1.15, s	1.15, s	1.05, s	1.27, s	0.98, s	1.06, s	0.87, s	0.88, s
20	1.23, s	1.13, s	1.12, s	1.12, s	1.22, s	1.29, s	1.24, s	1.21, s
1′								
2′								
OH-3			3.49, d (5.4)					
OH-6		3.29, br s	3.27, d (5.5)					
OH-7		4.14, br s						
OH-12	7.88, s	7.88, s	7.76, br s		6.18 br s	8.03, br s		
OCH_3-7						3.37, s		
$COCH_3$							2.01, s	
1′								3.77, t (4.9)
2′								3.54, t (4.9)
3′								3.43, t (5.4)
4′								1.52, m
5′								1.33, q (7.8)
6′								0.88, t (7.8)

[a] Acetone-d_6.
[b] Chloroform-*d*.

Table 2. The ^{13}C NMR data of compounds 1–3, 4a, and 5–8 in 125 MHz.

	1[a]	2[a]	3[a]	4a[b]	5[b]	6[b]	7[b]	8[b]
Position				δ_C				
1	40.2	40.1	37.8	37.1	37.8	40.8	35.9	35.7
2	19.8	19.9	28.6	20.1	18.9	20.2	18.6	18.9
3	44.5	44.0	78.9	42.5	41.3	42.5	41.1	41.0
4	34.3	34.3	40.4	71.6	33.3	34.4	33.0	33.1
5	54.3	53.0	57.9	51.1	49.3	54.2	46.1	45.3
6	75.0	70.6	67.9	34.8	36.0	62.2	24.7	23.0
7	79.0	70.3	40.6	197.9	198.4	74.4	64.7	70.0
8	129.2	128.5	126.2	124.6	124.2	127.6	137.7	139.8
9	148.2	148.2	148.5	155.3	157.0	148.7	153.9	151.8
10	40.6	39.3	38.6	38.6	38.1	43.6	39.1	39.1
11	110.5	110.2	110.1	110.1	110.3	115.3	187.8	188.3
12	154.4	154.6	153.4	158.3	157.9	154.4	132.0	131.6
13	133.1	132.7	132.2	132.9	127.0	132.0	153.5	153.6
14	126.4	126.9	127.0	126.7	127.8	132.9	186.0	187.1
15	27.6	27.6	27.4	26.8	141.2	27.4	26.4	26.4
16	22.9	22.9	23.0	23.3	116.2	22.7	21.2	21.2
17	23.0	23.0	23.0	22.4	24.2	22.9	21.3	21.3
18	36.8	35.7	29.9		32.6	35.3	33.0	33.0
19	22.5	22.6	16.9	22.6	21.4	24.0	21.6	21.9
20	26.9	24.7	23.0	23.0	23.2	23.4	18.8	18.6
$\underline{C}OCH_3$							169.6	
$CO\underline{C}H_3$							21.1	
OCH_3-7						58.0		
1′								69.4
2′								70.1
3′								71.0
4′								31.8
5′								19.3
6′								14.0

[a] Acetone-d_6.
[b] Chloroform-d.

presence of a hydroxy group and an aromatic ring, respectively. The maximum absorption of the UV spectrum at 235 and 280 nm also suggested the existence of an aromatic ring. The ^1H NMR spectrum in combination with HMQC spectrum of compound **1** showed two aromatic proton signals at δ_H 6.66 (1H, s, H-11), 7.28 (1H, s, H-14), a set of isopropyl group at δ_H 1.18 (3H, d, J = 6.9 Hz, H_3-16), 1.19 (3H, d, J = 6.9 Hz, H_3-17), 3.22 (1H, sep, J = 6.9 Hz, H-15), three methyl groups at δ_H 1.15 (3H, s, H_3-19), 1.23 (3H, s, H_3-18), 1.23 (3H, s, H_3-20), two oxymethines at δ_H 4.04 (1H, dd, J = 11.3, 7.2 Hz, H-6), 4.42 (1H, d, J = 7.2 Hz, H-7), and one hydroxy group at δ_H 7.88 (1H, s, OH-12, D_2O exchangeable) (Table 1). The ^{13}C NMR together with DEPT spectra of compound **1** showed an aromatic ring signals at δ_C 110.5 (C-11), 126.4 (C-14), 129.2 (C-8), 133.1 (C-13), 148.2 (C-9), 154.4 (C-12); five methyl signals at δ_C 22.5 (C-19), 22.9 (C-16), 23.0 (C-17), 26.9 (C-20), 36.8 (C-18); two oxymethine signals at δ_C 75.0 (C-6), 79.0 (C-7); three methylene signals at δ_C 19.8 (C-2), 40.2 (C-1), 44.5 (C-3); two methine signals at δ_C 27.6 (C-15), 54.3 (C-5); and one nonprotonated carbon signal at δ 40.6 (C-10) (Table 2). On account of unsaturated degree of an aromatic ring was four, indicating the existence of two additional rings to fit the six degrees of unsaturation in **1**. The COSY correlations of H_2-2/H_2-1 and H_2-3; H-6/H-5 and H-7 revealed the existence of two fragments, H-1-H-2-H-3 and H-5-H-6-H-7 (Fig. 2), respectively. Meanwhile, the isopropyl group was confirmed via cross-peaks of H-15/H_3-16 and H_3-17 in the COSY spectrum (Fig. 2). In the HMBC spectrum, the correlations of H-5/C-1, C-3, C-4, C-6, C-7, C-9, and C-10 verified the existence of a six-six-membered ring, and the correlations of H-7/C-8, C-9, and C-14 elucidated the aromatic ring was attached on C-8/C-9 (Fig. 2). Correlations of H-15/C-12, C-13, and C-14; H_3-16/C-13 in the HMBC spectrum indicated that the isopropyl group was connected to C-13, and the hydroxy group was attached on C-12 (Fig. 2). Further HMBC correlations of H_3-20/C-1, C-9, and C-10 supported that the methyl group (C-20) was located at C-10 (Fig. 2). Other key correlations of H-5/C-18 and C-19; H-18/C-3, C-4, C-5, and C-19 in the HMBC spectrum confirmed the dimethyl groups of C-18 and C-19 were located at C-4 (Fig. 2). Thus, the plain structures of compounds **1** and **2** were elucidated as 4β,5,6,7,8,8α,9,10-octahydro-4β,8,8-trimethyl-2-(1-methylethyl)-3,9,l0-phenanthrentriol, the same as that of 6β,7α-dihydroxyferruginol [24]. All spectroscopic data of individual compounds **1** and **2** indicated they were stereoisomers with the stereochemical centers at C-6/C-7. The relative configuration of H-5, H-6, and H-7 were confirmed by the coupling constant between H-5/H-6 and H-6/H-7 to be H_{ax}-5α, H_{ax}-6β, and H_{ax}-7β in compound **1** ($J_{H\text{-}5/H\text{-}6}$ = 11.3 Hz and $J_{H\text{-}6/H\text{-}7}$ = 7.2 Hz); H_{ax}-5α, H_{ax}-6β, and H_{eq}-7β in compound **2** ($J_{H\text{-}5/H\text{-}6}$ = 9.2 Hz and $J_{H\text{-}6/H\text{-}7}$ = 4.4 Hz), respectively. Meanwhile, the NOESY correlation between H-6/H-7 in compound **1**, H-5/H-7 in compound **2**, and the short of NOESY correlation between H-5/H-6 in both compounds **1** and **2** can proved the above concept (Fig. 3). The remaining chiral center of C-4 and C-10 in all compounds **1** and **2** were assigned to be H_{eq}-18α, H_{ax}-19β, and H_{ax}-20β based on the NOESY correlations of H-5/H_3-18 and H_3-19/H_3-20 (Fig. 3). Based on above assignments, the entire structures of compounds **1** and **2** were deduced to be as shown. Compounds **1** and **2** were previously unreported, and they were named as 6α,7β-dihydroxyferruginol and 6α,7α-dihydroxyferruginol, respectively.

Compound **3** was isolated as a gum with positive specific optical rotation, and displayed a molecular ion at m/z 318.2200 $[M]^+$ (calcd. 318.2189 for $C_{20}H_{30}O_3$) by HREIMS. The UV spectrum exhibited bands at 218 and 280 nm, indicating the presence of

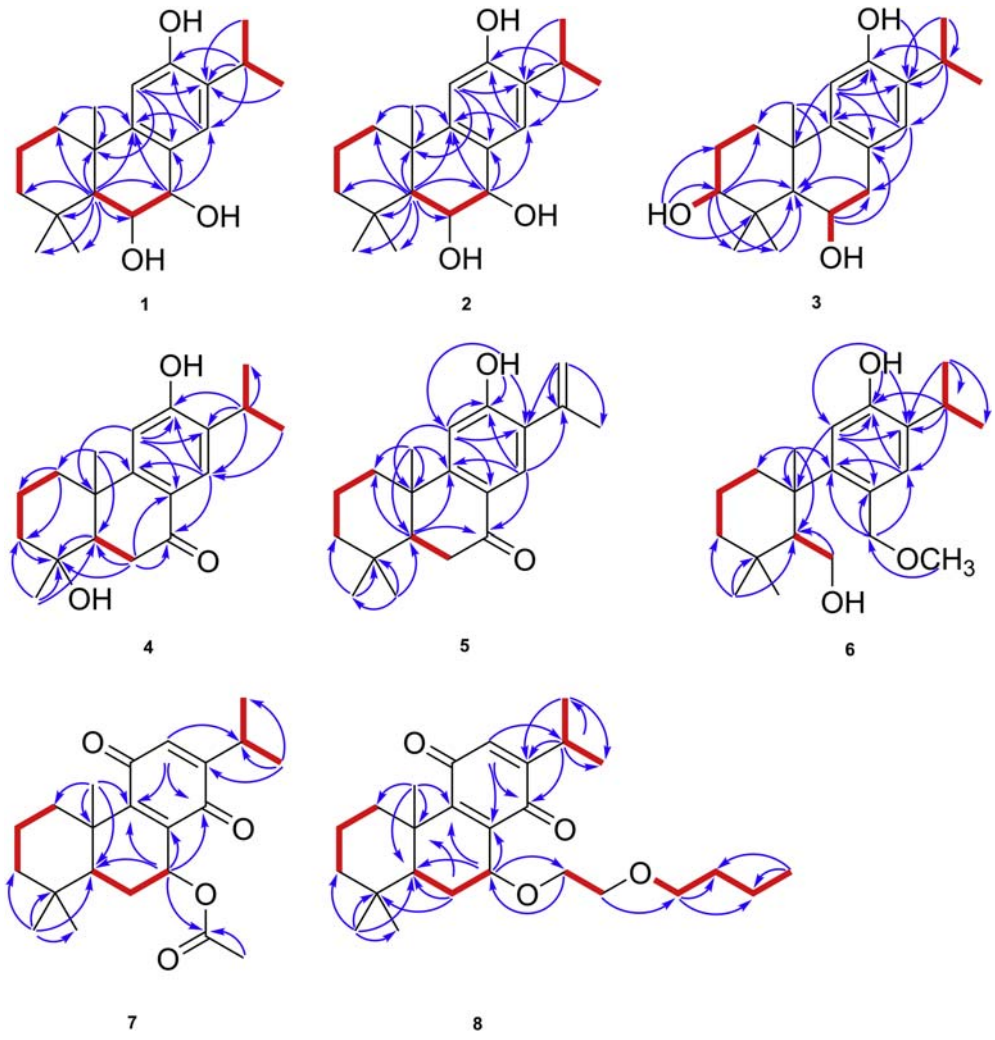

*Fig. 2. Key COSY (—) and HMBC (⟶) correlations of **1**–3, **4a**, and 5–8.*

an aromatic ring. The IR spectrum showed the absorption bands at 3368 cm^{-1} (hydroxy group), 1616, and 1505 cm^{-1} (aromatic ring). The NMR data of compound **3** were almost compatible with those of compound **1** except that the hydroxy group at C-7 in compound **1** was shifted to C-3 in compound **3** (Tables 1 and 2). The hydroxy group (δ_H 3.49, d, J = 5.4 Hz, O<u>H</u>-3, D_2O exchangeable) was located at C-3 based on the HMBC correlations of δ_H 3.18 (1H, m, H-3)/δ_C 37.8 (C-1), 57.9 (C-5), 29.9 (C-18), 16.9 (C-19) and δ_H 3.49 (O<u>H</u>-3)/δ_C 28.6 (C-2), 78.9 (C-3), and 40.4 (C-4) (Fig. 2). The NOESY correlations from δ_H 1.12 (3H, s, H_{ax}-20β) to δ_H 2.01 (1H, td, J = 12.6, 3.4 Hz, H_{eq}-1a), 4.31 (1H, m, H_{ax}-6β), and 1.05 (3H, s, H_{ax}-19β) indicated H-6, H-19, and H-20 were in β-axial position, and H-1a was in β-equatorial position (Fig. 3). Furthermore, H-3 occupied α-axial position based on the NOESY correlations from H-3 to δ_H 1.56 (1H, td, J = 12.6, 5.1 Hz, H_{ax}-1b), 1.15 (1H, m, H_{ax}-5α), and 1.20 (3H, s, H_{eq}-18α) (Fig. 3), and without NOESY correlation between H-3/H_{ax}-19β. Accordingly, the structure of compound **3** was well determined, and it was named 6α-hydroxyhinokiol.

Compound **4a** was assigned the molecular formula $C_{19}H_{26}O_3$ through analysis of its molecular ion $[M]^+$ at m/z 302.1881 (calcd. 302.1876), indicating seven degree of unsaturation. The existence of an aromatic ring was evidenced based on its UV λ_{max} at 231 and 281 nm and IR absorption bands at 1596, 1503, and 1461 cm^{-1}. The IR spectrum also revealed the hydroxy group (3335 cm^{-1}) and conjugated carbonyl group (1654 cm^{-1}). The NMR spectroscopic data of compound **4a** displayed similarity to those of sugiol (**4b**) [25] except that the methyl group (C-18) of **4b** was replaced by a hydroxy group in compound **4a** with down field shift of C-4 to δ_C 71.6. (Tables 1 and 2). The presence of the C-7 carbonyl group was indicated by the HMBC correlations from δ_H 2.08 (1H, dd, J = 14.1, 3.5 Hz, H-5), 2.55 (1H, dd, J = 17.9, 3.5 Hz, H-6b), 2.91 (1H, dd, J = 17.9, 14.1 Hz, H-6a) and 7.91 (1H,

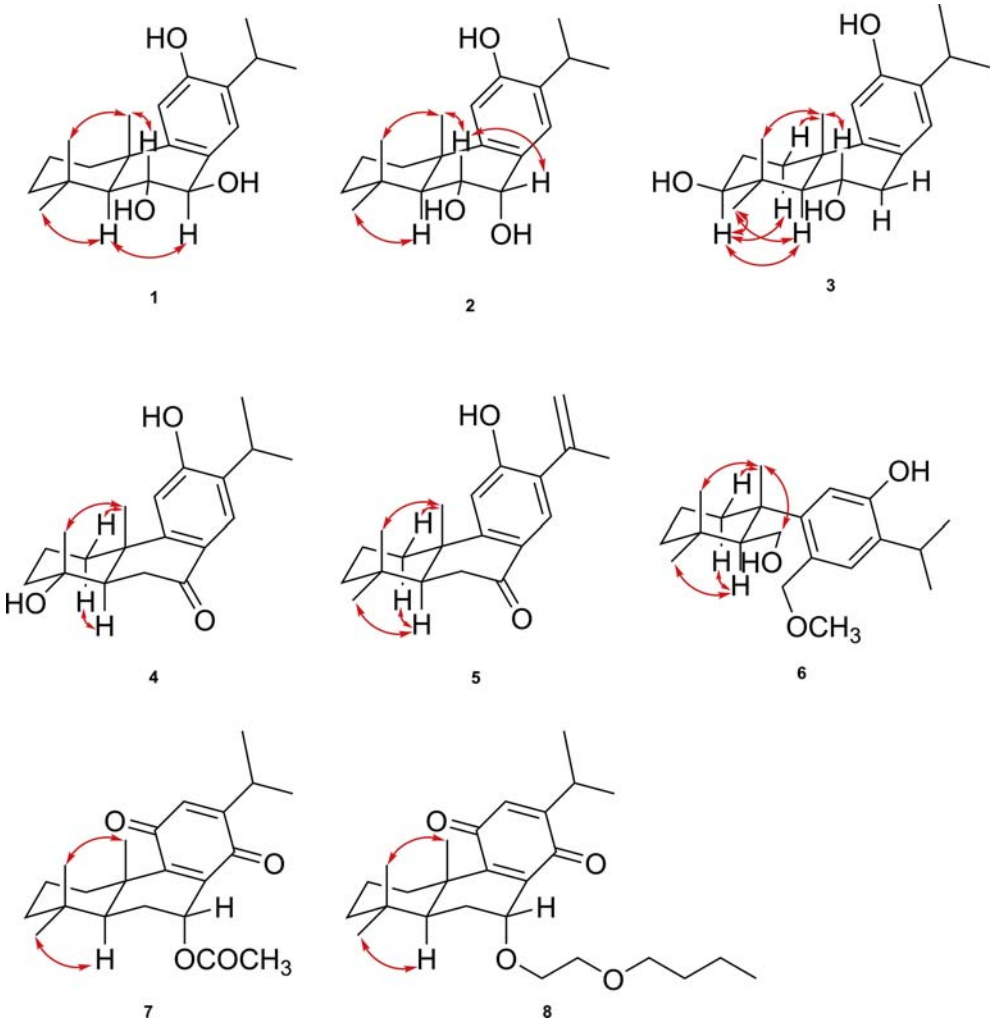

*Fig. 3. Key NOESY (↔) correlations of **1**–**3**, **4a**, and **5**–**8**.*

s, H-14) to C-7 (Fig. 2). The HMBC correlations from δ_H 1.41 (1H, td, $J = 13.4, 3.7$ Hz, H-3b), 2.08 (H-5), 2.55 (H-6), and 1.27 (3H, s, H-19) to δ_C 71.6 (C-4) confirmed a hydroxy group was attached at C-4 (Fig. 2). The NOESY correlations of H_{ax}-20 (δ 1.12)/H_{eq}-1a (δ 2.16) and H_{ax}-19 (δ 1.27); H_{ax}-5/H_{ax}-1b (Fig. 3), corroborated that H-19 and H-20 were in β-position, while OH-4 and H-5 were in α-position. Consequently, compound **4a** was identified as 4α-hydroxy-7-oxo-18-norabieta-8,11,13-triene-4α-ol.

The physical data and spectroscopic properties of compound **5** were almost identical with that of sugiol (**4b**), except the isopropyl group in compound **4b** was replaced by the isopropenyl in compound **5**. The methyl group of **5** at δ_H 0.91 (3H, s, H_3-18) was attached on C-4 (δ_C 33.3) based on the HMBC correlations of δ_H 0.91 (3H, s, H_3-18)/δ_C 33.3 (C-4), 49.3 (C-5), and 21.4 (C-19) (Fig. 2). Regarding the compound **5**, the terminal alkene [υ_{max} 898, 870 cm^{-1} in IR spectrum] [δ_H 5.11 (1H, br s, H-16b) and 5.41 (1H, br s, H-16a); δ_C 116.2 (C-16) and 141.2 (C-15)] was assigned for C-15 and C-16 based on the HMBC correlations of H_2-16/C-14, C-15, C-17 and H-14/C-15 (Fig. 2). The relative configuration of compound **5** was identical to those of compound **4b** based on their similar NOESY spectroscopic data (Fig. 3). The structure of compound **5** were thus established as shown, and was named 15,16-dehydrosugiol.

Compound **6** was obtained as a colorless solid, and its molecular formula was established as $C_{21}H_{34}O_3$ by HREIMS with a molecular ion $[M]^+$ at *m/z* 334.2503 (calcd. 334.2509), which was consistent with five indices of hydrogen deficiency (IHDs). The IR spectrum showed a hydroxy group (3368 cm^{-1}) and an aromatic ring (1614, 1582, 1485 cm^{-1}), which was also reflected in its UV absorbance maxima at 231 and 281 nm. The ^{13}C NMR and DEPT data of **6** were very similar to those of **1** with the exception that resonances associated with the oxymethines (C-6 and C-7) in **1** were changed into two oxymethylene

groups [δ 62.2 (C-6) and 74.4 (C-7)] in **6** (Table 2). Besides, the NMR spectra of **6** showed an additional methoxy group [δ_H 3.37 (3H, s, -OCH_3); δ_C 58.0 (-OCH3)] (Tables 1 and 2). These results, together with the five IHDs, indicated that **6** was proposed being 6,7-secoabietane diterpene. The ^{1}H-^{1}H COSY plot between δ_H 2.17 (1H, m, H-5) and δ_H 3.40 (1H, m, H-6b)/3.55 (1H, br s, H-6a) (Fig. 2), as well as the intense HMBC correlation from H_2-6 to δ_C 54.2 (C-5) (Fig. 2), indicating the connectivity between C-5 and C-6. The connection between C-7 and C-8 was confirmed by the HMBC correlations from δ_H 4.57 (1H, br d, J = 10.4 Hz, H-7b)/4.70 (1H, d, J = 10.4 Hz, H-7a) to δ_C 127.6 (C-8), 132.9 (C-14), and 148.7 (C-9) (Fig. 2). The methoxy group (3.37, s, −OCH_3) located at C-7 was demonstrated by the HMBC correlation from −OCH_3 to C-7 (Fig. 2). The relative configuration of **6** was established by interpretation of its NOESY spectrum, in which the cross-peak of δ_H 1.29 (3H, s, H_{ax}-20β)/δ_H 3.40, 3.55 (each 1H, H_{eq}-6β) and 1.06 (3H, s, H_{ax}-19β) (Fig. 3), and the absence of NOESY correlation between δ_H 2.17 (1H, m, H_{ax}-5α)/δ_H 1.29 (3H, s, H_{ax}-20β), indicating H-6, H-19, and H-20 were in β-orientation, while H-5 was in the opposite site. Therefore, compound **6** was identified as shown, and was named 7-methoxy-6,7-secoabieta-8,11,13-triene-6,12-diol.

Compound **7** was a yellowish solid with molecular formula $C_{22}H_{30}O_4$ determined from HREIMS with a molecular ion $[M]^+$ at *m/z* 358.2151 (calcd. 358.2145). Maximal UV absorption at 257 nm, IR absorptions at 1731, 1650, and 1603 cm^{-1}, as well as the ^{13}C NMR peaks (Table 2) at δ132.0 (C-12), 137.7 (C-8), 153.5 (C-13), 153.9 (C-9), 186.0 (C-14), and 187.8 (C-11) suggested the existence of *p*-benzoquinone residue [26]. Typical ^{1}H NMR spectrum (Table 1) of an isopropyl signals at δ 1.07 (3H, d, J = 6.8 Hz, H-16), 1.09 (3H, J = 6.8 Hz, H-17), 2.97 (1H, sep, J = 6.8 Hz, H-15) and three singlet methyl signals at δ 0.85 (3H, s, H-18), 0.87 (3H, s, H-19), 1.24 (3H, s, H-20) revealed compound **7** was an abietane diterpene. Based on the above data, compound **7** was almost compatible with the known compound, 12-deoxyroyleanone [26], except that the molecular weight of compound **7** were 58 Da ($C_2H_2O_2$) more than that of 12-deoxyroyleanone, indicating that compound **7** was the acetoxy derivative of 12-deoxyroyleanone. Further HMBC correlations (Fig. 2) from H-7 [δ_H 5.91 (d, J = 4.1 Hz)] to acetoxy group (δ_C 169.6) confirmed the acetoxy group was located at C-7. Besides, compound **7** had smaller coupling constant (J = 4.1 Hz) between H-6/H-7 as well as the NOESY cross-peak (Fig. 3) between δ_H 5.91 (1H, d, J = 4.1 Hz, H-7) and δ_H 1.63 (1H, td, J = 14.9, 4.1 Hz, H_{ax}-6β)/1.92 (1H, d, J = 14.9 Hz, H_{eq}-6α) determining that H-7 was in β-equatorial orientation. After fully assignments, compound **7** was named 7α-acetoxyabieta-8,12-diene-11,14-dione.

Compound **8** was yield as a yellowish solid and assign the molecular formula $C_{26}H_{40}O_4$ through analysis of its HREIMS data. The physical data and NMR spectroscopic spectra of **8** were similar to those of compound **7** (Tables 1 and 2), except for the acetoxy group in **7** was replaced by the ether-linkage alkyl side chain in **8**. The ether-linkage alkyl side chain was confirmed by the COSY correlations of δ_H 3.77 (2H, t, J = 4.9 Hz, H-1′)/3.54 (2H, t, J = 4.9 Hz, H-2′) and δ_H 3.43 (2H, t, J = 5.4 Hz, H-3′)/1.52 (2H, m, H-4′)/1.33 (2H, q, J = 7.8 Hz, H-5′)/0.88 (3H, t, J = 7.8 Hz, H-6′) (Fig. 2), as well as the HMBC correlations from H-2′ to δ_C 71.0 (C-3′); H-6′ to δ_C 31.8 (C-4′) and 19.3 (C-5′); and H-3′ to C-4′ (Fig. 2). In the HMBC spectrum, distinctive plot-spot of δ_H 4.41 (1H, br d, J = 3.6 Hz, H-7) to δ_C 69.4 (C-1′) indicated the alkyl side chain was attached to C-7 (Fig. 2). The small coupling constant between H-7 and H-6 (br d, J = 3.6 Hz) and the absent of NOESY correlation of H_{ax}-5α/H-7 indicated H-7 was in β-equatorial position. Accordingly, the entire structure of **8** was established, and it was named 7α-butyloxyethyloxyabieta-8,12-diene-11,14-dione.

By comparing the spectroscopic data ($[\alpha]_D$, UV, IR, NMR and MS) of known compounds with the literature data, the known diterpenes were identified to be 6,7-dehydroferruginol (**9**) [24], 12-hydroxy-6,7-secoabieta-8,11,13-triene-6,7-dial (**10**) [27], 7α-11-dihydroxy-12-methoxy-8,11,13-abietatriene (**11**) [28], and 11,14-dihydroxy-8,11,13-abietatrien-7-one (**12**) [29].

We evaluated anti-lymphangiogenesis potentials of four isolates (**9**, **10**, **11**, and **12**) present in sufficient amounts in human lymphatic endothelial cells (LECs). Lymphangiogenesis is the process forming new lymphatic vessels emerge from pre-existent vessels or post-capillary venules. Most of lymphangiogenesis occurs in pathologic inflammatory conditions, especially in tumor conditions. Therefore, anti-lymphangiogenesis can stop tumor cells spread in the regional lymph nodes and constitute a therapeutic target for anti-cancer. As shown in

Table 3. Anti-lymphangiogenic effects of selected compounds.

Compound	IC_{50} (μM)
9	47 ± 1
10	18 ± 2
11	33 ± 2
12	36 ± 2
Rapamycin	<10

LECs were treated with the indicated compounds for 48 h, and anti-lymphangiogenic effects were elucidated in a cell growth assay (n = 3). Data are expressed as the mean ± SEM. Rapamycin was used as a positive control.

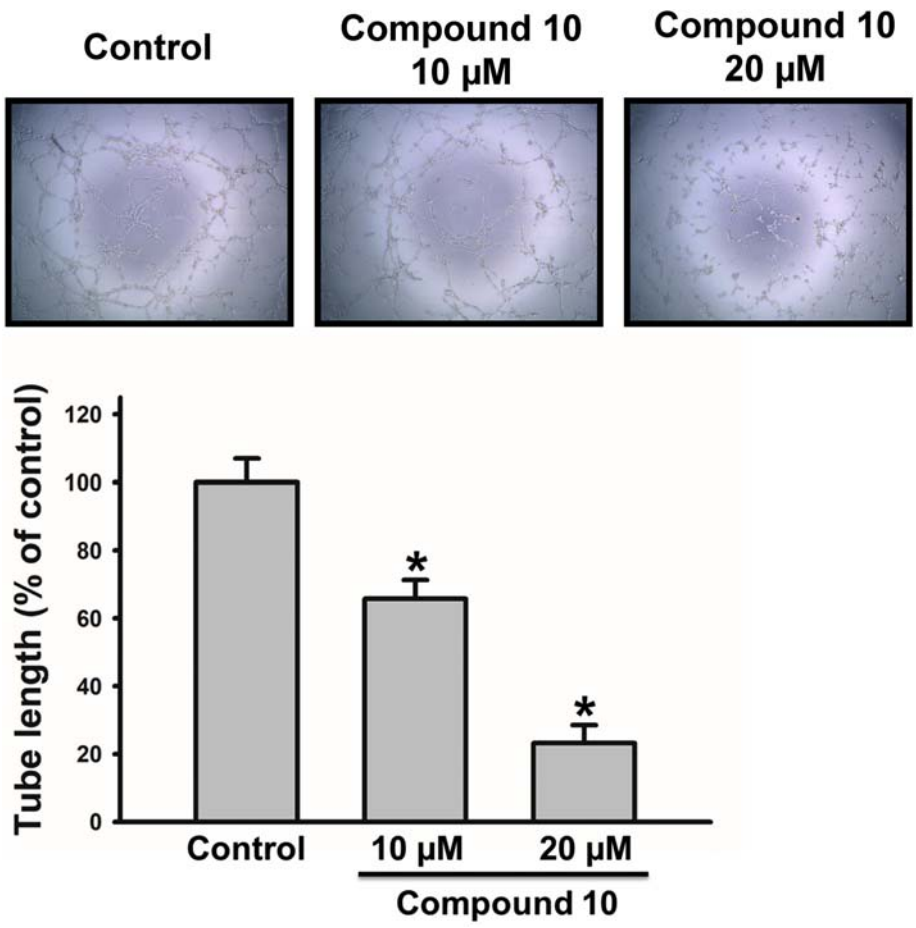

*Fig. 4. Effect of compound **10** on LEC tube formation. Cells were treated with compound **10** (10 μM and 20 μM, respectively) for 8 h. Capillary-like structure formation was examined by a tube formation assay (n = 5). Tube formation of LECs was quantified by measuring the length of tubes using Image software. Data are expressed as the mean ± SEM. *p < 0.05 compared with the control (CTL) group.*

Table 3, 12-hydroxy-6,7-secoabieta-8,11,13-triene-6,7-dial (**10**) exhibited the most potent anti-lymphangiogeneic activity by suppressing LECs growth (IC_{50} = 18 ± 2 μM), with rapamycin as the positive control. 6,7-Dehydroferruginol (**9**), 7α-11-dihydroxy-12-methoxy-8,11,13-abietatriene (**11**), and 11,14-dihydroxy-8,11,13-abietatrien-7-one (**12**) illustrated moderate growth-inhibitory effects on LECs with IC_{50} values of 47 ± 1, 33 ± 2, and 36 ± 2 μM, respectively. Capillary-like tubules are regarded as an important physiological phenomenon of lymphangiogenesis. For confirming the anti-lymphangiogeic effects of the active compounds, the tube formation assay was performed. As shown in Fig. 4 compound **10** significantly repressed LECs tube formation in a concentration-dependent manner (IC_{50} = 13.8 ± 0.6 μM). In addition, we found that compound **10** did not induce the significant lactate dehydrogenase (LDH) release in LECs (Suppl. Fig. S1). These findings suggested that compound **10** display the anti-lymphangiogenesis property without any signs of cytotoxicity.

Based on the anti-lymphangiogenesis results, the structure-activity-relationship (SAR) study depicted that the 6,7-*seco*-abietane type diterpene (compound **10**) can considerably increase anti-lymphangiogenic activity. The close IC_{50} values of **11** and **12** depict the substituted might not influence the activity. Among aromatic abietane diterpenes **9**, **11**, and **12**, compounds **11** and **12** showed better LECs growth inhibition activity than compound **9**. This finding suggested that the unsaturation between C6-C7 may decrease anti-lymphangiogenic activity.

Declaration of competing interest

The authors declare no conflicts of interest.

Acknowledgments

This work was financially supported by China Medical University grant in Taichung, Taiwan (CMU110-Z-08 and CMU109-AWARD-02) and "Chinese Medicine Research Center, China Medical

University, Taichung, Taiwan" from The Featured Areas Research Center Program within the framework of the Higher Education Sprout Project by the Ministry of Education (MOE) in Taipei, Taiwan (CMRC-CHM-2-1).

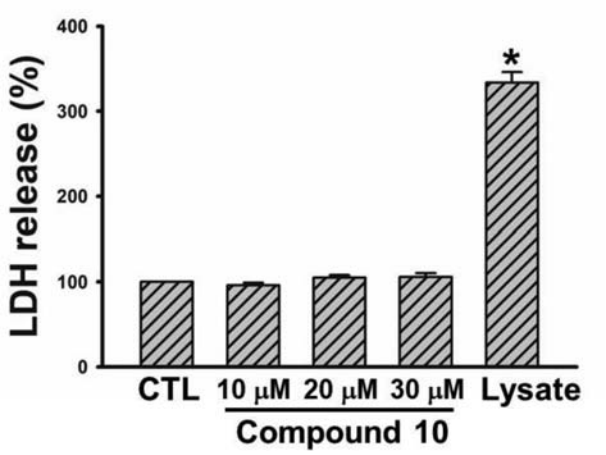

*Fig. S1. Effect of compound **10** on cytotoxicity of LECs. Cells were treated with the indicated concentrations of compound 10 for 8 h; then the cytotoxicity was evaluated by the LDH assay (n = 3). Data are expressed as the mean ± SEM. *p < 0.05 compared with the control (CTL) group.*

~~Appendix.~~

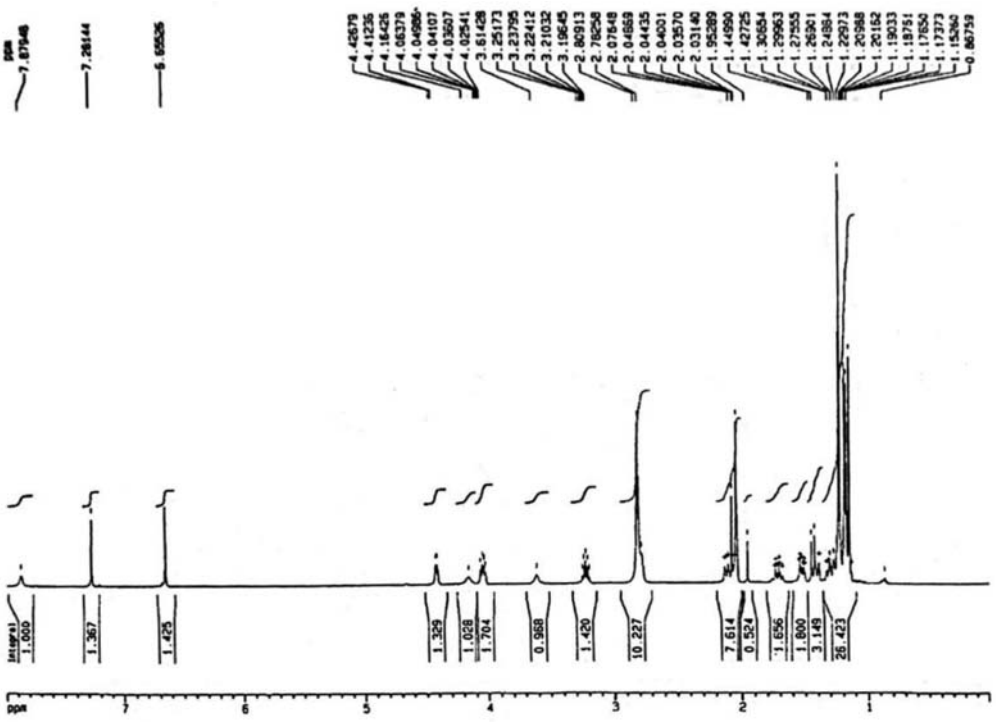

*Fig. S2. ^{1}H NMR spectrum of 6α,7β-dihydroxyferruginol (**1**) in acetone-d_6 at 500 MHz.*

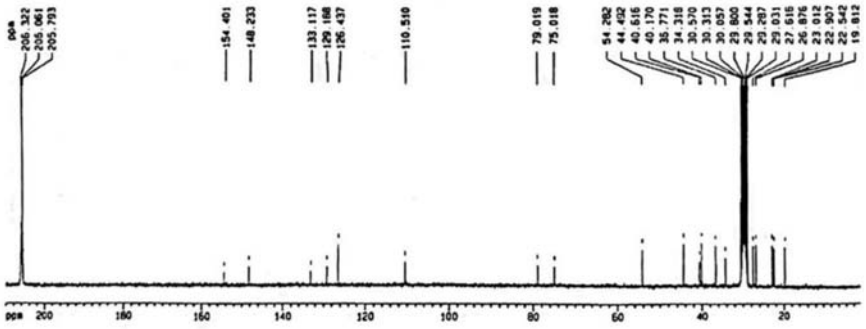

Fig. S3. ^{13}C *NMR spectrum of 6α,7β-dihydroxyferruginol (**1**) in acetone-*d_6 *at 125 MHz.*

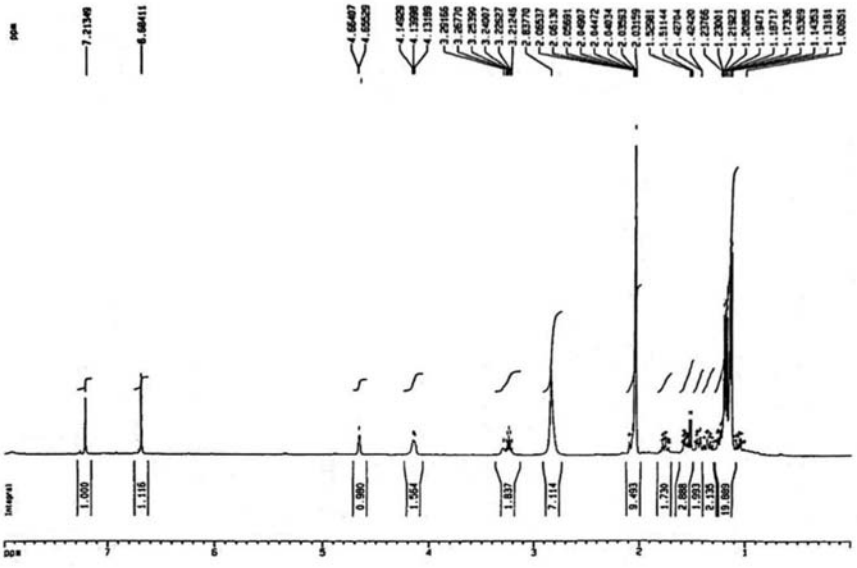

Fig. S4. ^{1}H *NMR spectrum of 6α,7α-dihydroxyferruginol (**2**) in acetone-*d_6 *at 500 MHz.*

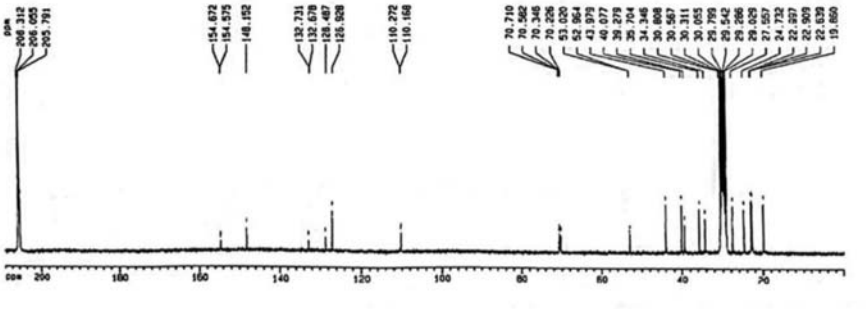

Fig. S5. ^{13}C *NMR spectrum of 6α,7α-dihydroxyferruginol (**2**) in acetone-*d_6 *at 125 MHz.*

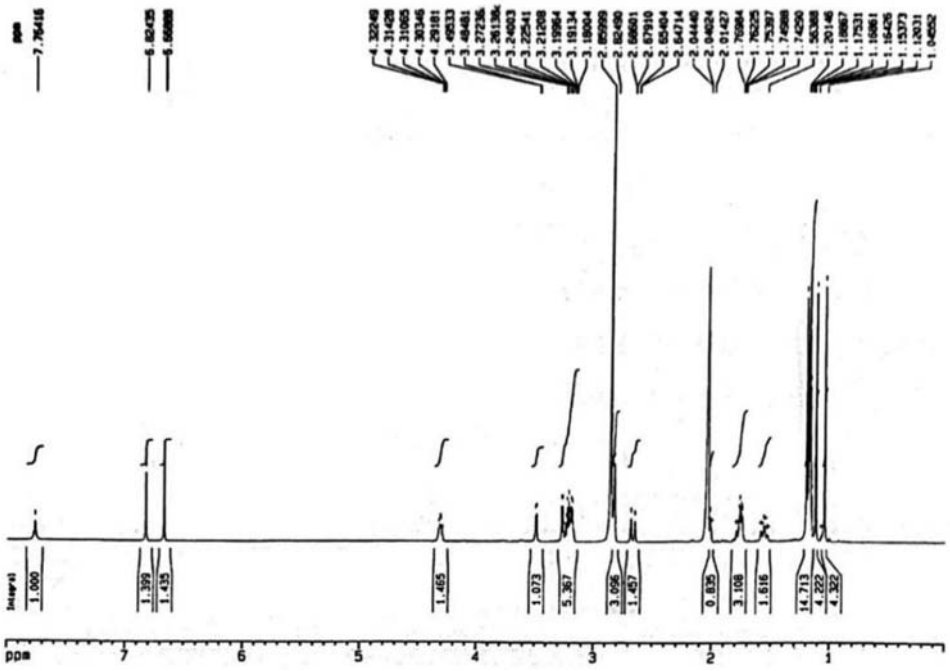

*Fig. S6. ^{1}H NMR spectrum of 6α-hydroxyhinokiol (**3**) in acetone-d_6 at 500 MHz.*

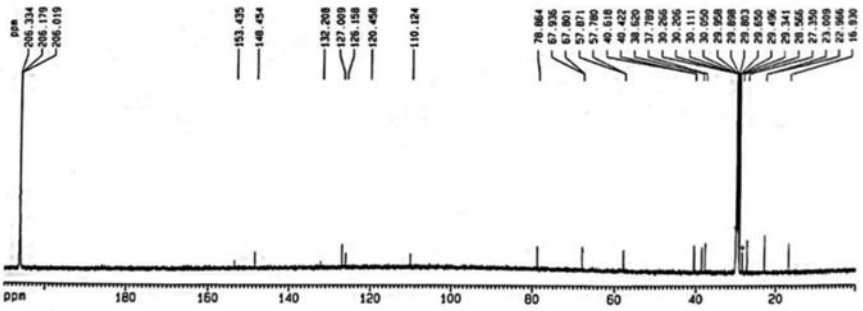

*Fig. S7. ^{13}C NMR spectrum of 6α-hydroxyhinokiol (**3**) in acetone-d_6 at 125 MHz.*

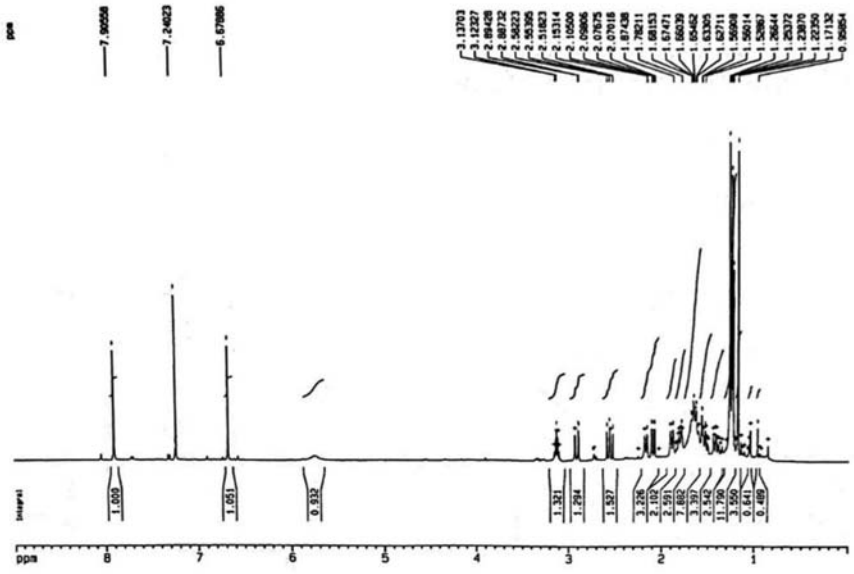

*Fig. S8. ^{1}H NMR spectrum of 4α-hydroxy-7-oxo-18-norabieta-8,11,13-triene-4α-ol (**4a**) in CDCl3 at 500 MHz.*

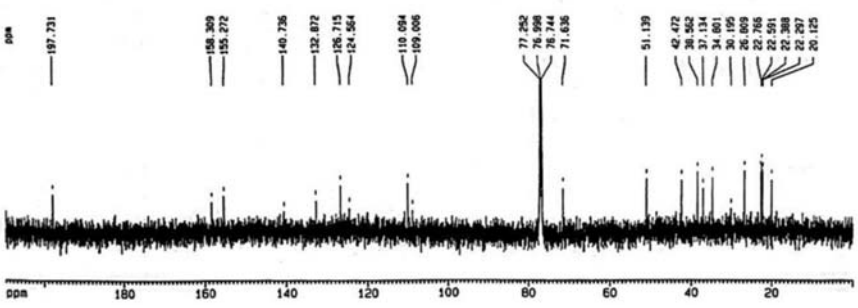

*Fig. S9. ^{13}C NMR spectrum of 4α-hydroxy-7-oxo-18-norabieta-8,11,13-triene-4α-ol (**4a**) in CDCl3 at 125 MHz.*

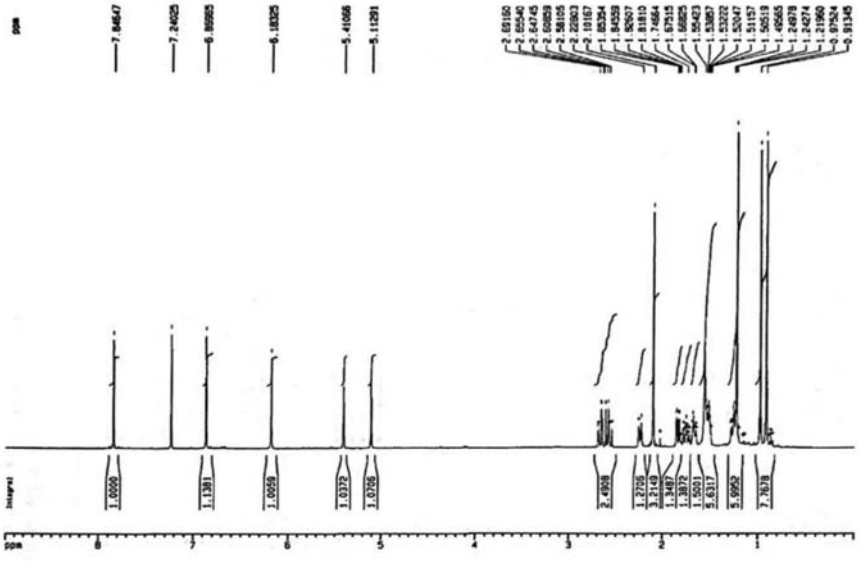

*Fig. S10. ^{1}H NMR spectrum of 15,16-dehydrosugiol (**5**) in $CDCl_3$ at 500 MHz.*

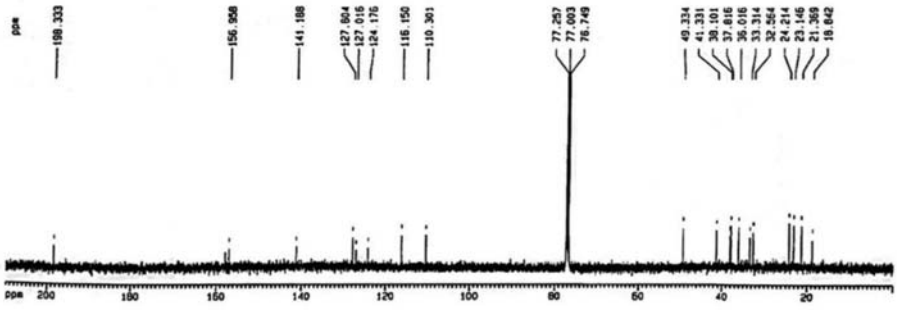

*Fig. S11. ^{13}C NMR spectrum of 15,16-dehydrosugiol (**5**) in $CDCl_3$ at 125 MHz.*

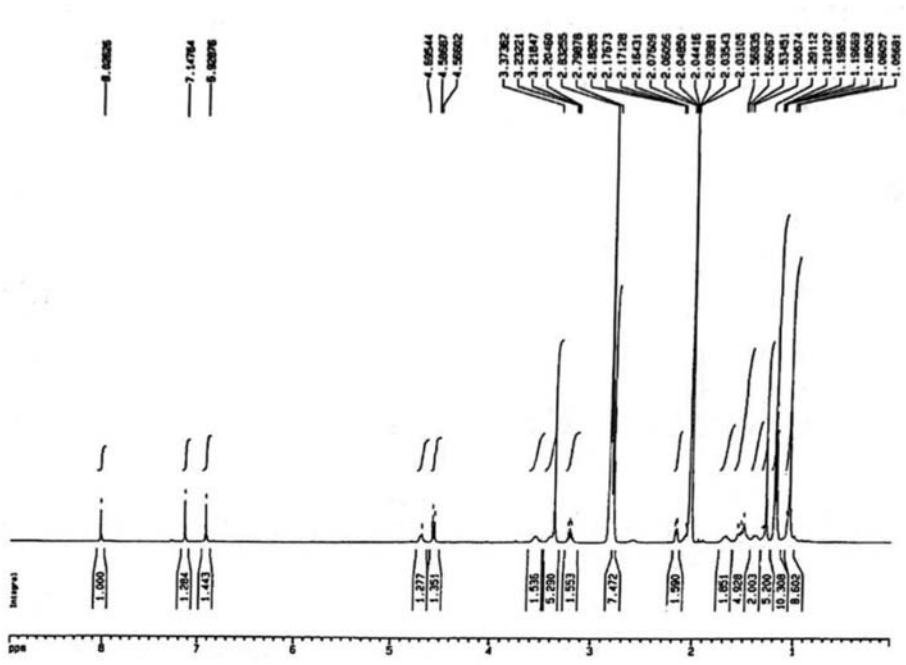

*Fig. S12 ^{1}H NMR spectrum of 7-methoxy-6,7-secoabieta-8,11,13-triene-6,12-diol (**6**) in $CDCl_3$ at 500 MHz.*

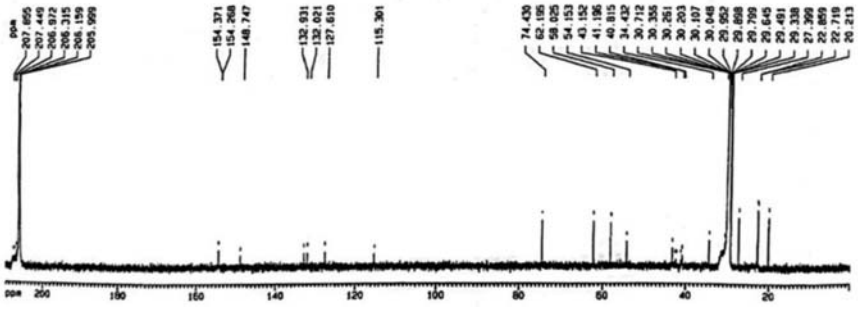

*Fig. S13. ^{13}C NMR spectrum of 7-methoxy-6,7-secoabieta-8,11,13-triene-6,12-diol (**6**) in $CDCl_3$ at 125 MHz.*

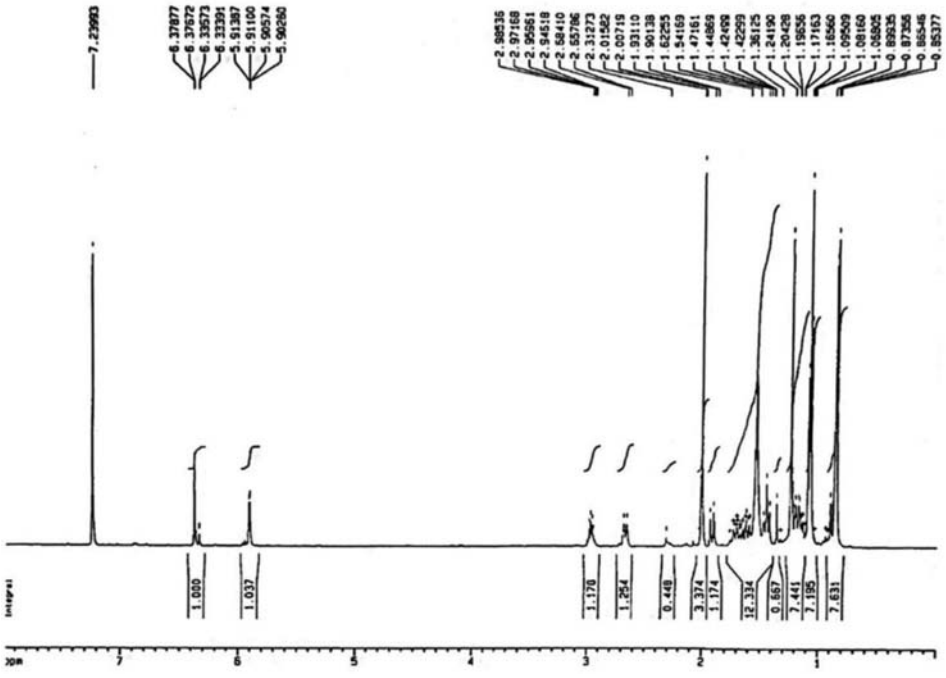

*Fig. S14. ^{1}H NMR spectrum of 7α-acetoxyabieta-8,12-diene-11,14-dione (**7**) in $CDCl_3$ at 500 MHz.*

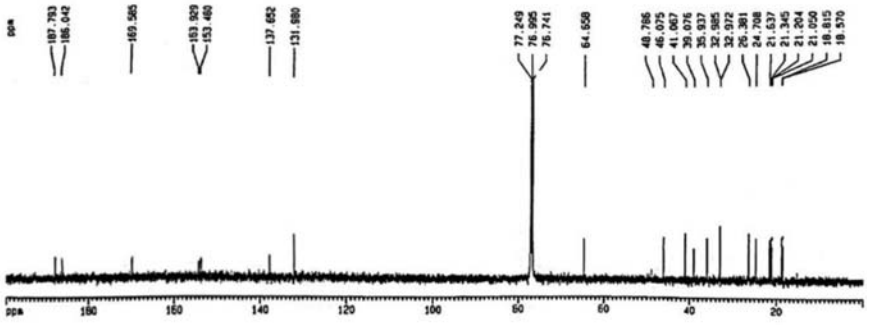

Fig. S15 ^{13}C NMR spectrum of 7α-acetoxyabieta-8,12-diene-11,14-dione (7) in $CDCl_3$ at 125 MHz.

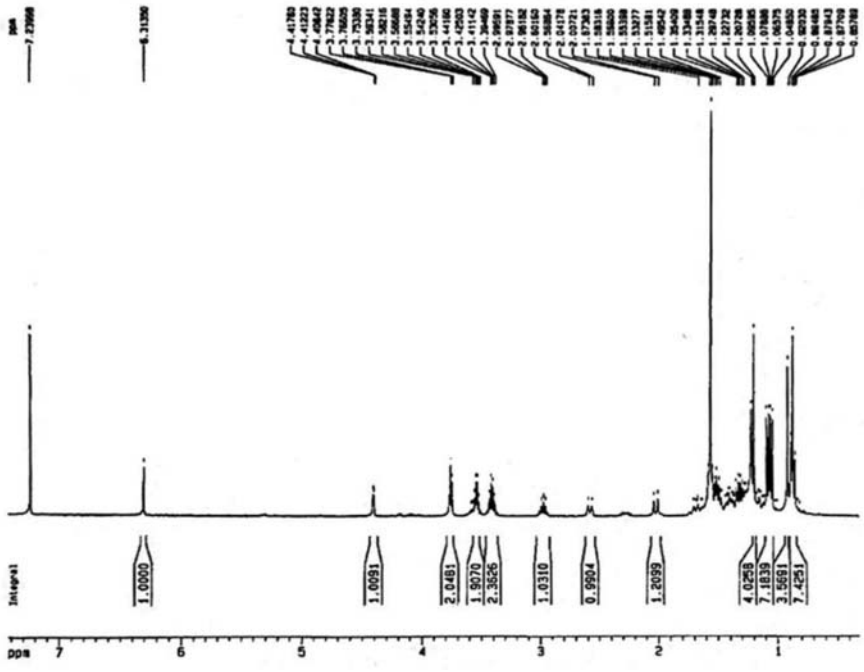

Fig. S16. ^{1}H NMR spectrum of 7α-butyloxyethyloxyabieta-8,12-diene-11,14-dione (8) in $CDCl_3$ at 500 MHz.

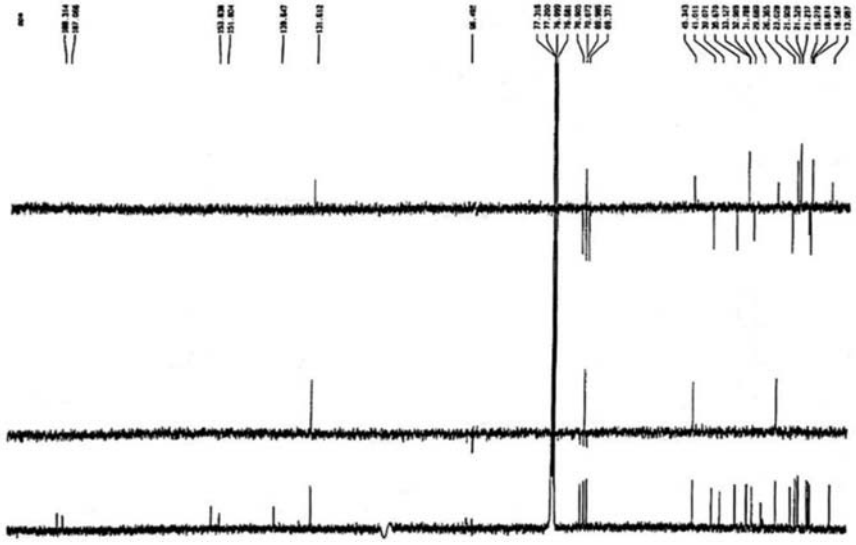

Fig. S17. DEPT spectrum of 7α-butyloxyethyloxyabieta-8,12-diene-11,14-dione (8).

References

[1] Oh CM, Lee D, Kong HJ, Lee S, Won YJ, Jung KW, et al. Causes of death among cancer patients in the era of cancer survivorship in Korea: attention to the suicide and cardiovascular mortality. Cancer Med 2020;9:1741–52.

[2] Paduch R. The role of lymphangiogenesis and angiogenesis in tumor metastasis. Cell Oncol 2016;39:397–410.

[3] Shirouzu T, Watari K, Ono M, Koizumi K, Saiki I, Tanaka C, et al. Structure, synthesis, and biological activity of a C-20 bisacetylenic alcohol from a marine sponge *Callyspongia* sp. J Nat Prod 2013;76:1337–42.

[4] Wu XD, Wang SY, Wang L, He J, Li GT, Ding LF, et al. Labdane diterpenoids and lignans from *Calocedrus macrolepis*. Fitoterapia 2013;85:154–60.

[5] Wang SY, Wu JH, Cheng SS, Lo CP, Chang HN, Shyur LF, et al. Antioxidant activity of extracts from *Calocedrus formosana* leaf, bark, and heartwood. J Wood Sci 2004;50:422–6.

[6] Inamori Y, Sakagami Y, Morita Y, Shibata M, Sugiura M, Kumeda Y, et al. Antifungal activity of hinokitiol-related compounds on wood-rotting fungi and their insecticidal activities. Biol Pharm Bull 2000;23:995–7.

[7] Lo TB, Lin YT. Study on the extractive constituents from the wood of *libocedrus formosana*, Florin. I. Chin Chem Soc 1956;3: 30–5.

[8] Lin YT, Lin KT, Wang KT, Weinstein B. Phytochemical studies. Isolation of 5-ethyltropolone from *Libocedrus formosana*. Experientia 1966;22:140–1.

[9] Ichikawa N. Studies on the constitution of shonanic acid, one of the two characteristic volatile acids from the wood of *Libocedrus formosana*, Florin. V. Studies on the oxidation of dihydroshonanyl alcohol and the ozonolysis of shonanic acid. Bull Chem Soc Jpn 1937;12:258–66.

[10] Lee TH, Lee MS, Ko HH, Chen JJ, Chang HS, Tseng MH, et al. New furanone and sesquiterpene from the pericarp of *Calocedrus formosana*. Nat Prod Commun 2015;10:845–6.

[11] Hsieh CL, Shiu LL, Tseng MH, Shao YY, Kuo YH. Calocedimers A, B, C, and D from the bark of *Calocedrus macrolepis* var. *formosana*. J Nat Prod 2006;69:665–7.

[12] Lin YT, Liu KT. A study of the extractive constiuents from the wood of *Libocedrus Formosana*, Florin. VIII. The phenolic components. Shonanol, a new diterpene phenol. Chin Chem Soc 1965;12:51–60.

[13] Hsieh CL, Tseng MH, Pan RN, Chang JY, Kuo CC, Lee TH, et al. Novel terpenoids from *Calocedrus macrolepis* var. *formosana*. Chem Biodivers 2011;8:1901–7.

[14] Hsieh YH, Chen KJ, Chien SC, Cheng WL, Xiao JH, Wang SY. ACAT inhibitory activity of exudates from *Calocedrus macrolepis* var. *formosana*. Nat Prod Commun 2012;7. 1934578X1200701206.

[15] Hsieh CL, Tseng MH, Kuo YH. Formosadimers A, B, and C from the bark of *Calocedrus macrolepis* var. *formosana*. Chem Pharm Bull 2005;53:1463–5.

[16] Hsieh CL, Tseng MH, Shao YY, Chang JY, Kuo CC, Chang CY, et al. C35 terpenoids from the bark of *Calocedrus macrolepis* var. *formosana* with activity against human cancer cell lines. J Nat Prod 2006;69:1611–3.

[17] Hsien CL, Tseng MH, Pan RN, Chang JY, Kuo CC, Lee TH, et al. Labdanecaryophyllic acid, a novel cytotoxic C35 terpenoid from *Calocedrus macrolepis* var. *formosana*. Tetrahedron Lett 2011;52:515–7.

[18] Ho ST, Lin CC, Wu TL, Tung YT, Wu JH. Antitumor agent yatein from *Calocedrus formosana* Florin leaf induces apoptosis in non-small-cell lung cancer cells. J Wood Sci 2019;65:59.

[19] Chao LK, Hua KF, Hsu HY, Su YC, Chang ST. Bioactivity assay of extracts from *Calocedrus macrolepis* var. *formosana* bark. Bioresour Technol 2006;97:2462–5.

[20] Ho CL, Tseng YH, Wang EI, Liao PC, Chou JC, Lin CN, et al. Composition, antioxidant and antimicrobial activities of the seed essential oil of *Calocedrus formosana* from Taiwan. Nat Prod Commun 2011;6:133–6.

[21] Chang HT, Cheng YH, Wu CL, Chang ST, Chang TT, Su YC. Antifungal activity of essential oil and its constituents from *Calocedrus macrolepis* var. *formosana* Florin leaf against plant pathogenic fungi. Bioresour Technol 2008;99:6266–70.

[22] Chang FR, Wang SW, Chen SR, Lee CY, Sheu JH, Cheng YB. Aleuritin, a novel dinor-diterpenoid from the twigs of *Aleurites moluccanus* with an anti-lymphangiogenic effect. Org Biomol Chem 2020;18:7892–8.

[23] Chen SR, Wang SW, Chang FR, Cheng YB. Anti-lymphangiogenic alkaloids from the zoanthid *Zoanthus vietnamensis* collected in taiwan. J Nat Prod 2019;82:2790–9.

[24] Haslinger E, Michl G. Synthese von (+)-taxodion. Liebigs Annalen der Chemie 1989;1989:677–86.

[25] Chao KP, Hua KF, Hsu HY, Su YC, Chang ST. Anti-inflammatory activity of sugiol, a diterpene isolated from *Calocedrus formosana* bark. Planta Med 2005;71:300–5.

[26] Tan N, Kaloga M, Radtke OA, Kiderlen AF, Öksüz S, Ulubelen A, et al. Abietane diterpenoids and triterpenoic acids from *Salvia cilicica* and their antileishmanial activities. Phytochemistry 2002;61:881–4.

[27] Nasipuri D, Guha M. 821. Synthetical studies in the diterpene series. Part II. Synthesis of (±)-sugiyl methyl ether and related compounds. J Chem Soc 1962:4248–52.

[28] Valverde S, Escudero J, Cristóbal López J, Ma Rabanal R. Two terpenoids from *Salvia bicolor*. Phytochemistry 1985;24: 111–3.

[29] Kuo YH, Chen CH, Huang SL. New diterpenes from the heartwood of *Chamaecyparis obtusa* var. *formosana*. J Nat Prod 1998;61:829–31.